

Author Manuscript

Title: Exploring the Role of Organic Functional Groups in the Ionothermal Synthesis of Uranyl Phosphate Materials

Authors: Tsuyoshi A. Kohlgruber; Daniel E. Felton; Hrafn Traustason; Peter C Burns, Ph.D.

This is the author manuscript accepted for publication. It has not been through the copyediting, typesetting, pagination and proofreading process, which may lead to differences between this version and the Version of Record.

To be cited as: 10.1002/zaac.202200162

Link to VoR: <https://doi.org/10.1002/zaac.202200162>

Exploring the Role of Organic Functional Groups in the Ionothermal Synthesis of Uranyl Phosphate Materials

Tsuyoshi A. Kohlgruber,¹ Daniel E. Felton,² Hrafn Traustason,² Peter C. Burns^{1,2}*

¹ Department of Civil and Environmental Engineering and Earth Sciences, University of Notre Dame, Notre Dame, IN, 46556, USA.

² Department of Chemistry and Biochemistry, University of Notre Dame, Notre Dame, IN, 46556, USA.

*email: pburns@nd.edu

Author Manuscript

Abstract

Four new hybrid organic-inorganic uranyl phosphate compounds were structurally characterized after single crystals were grown via ionothermal synthesis using the ionic liquids 1-ethyl-3-methylimidazolium dimethyl phosphate and 1-ethyl-3-methylimidazolium dibutyl phosphate. Three of the new crystal structures presented here incorporate dimethyl or monomethyl phosphate ligands into the structural unit to form one chain-based compound and two sheet-based compounds. One of the structures utilizes dibutyl phosphate to form a previously reported uranyl compound, a structural polymorph that crystallized in space group $P2_1/c$ in contrast to the previously reported $P-1$ structure. The structural and topological relationships are compared to those of uranyl phosphate minerals as well as previously reported organophosphate compounds. The roles of the organics on the phosphate anions in impacting uranyl coordination and stabilizing the crystal structures are discussed.

Keywords: Uranyl; Organophosphate; X-ray diffraction; Ionic liquid; Coordination

1. Introduction

Hexavalent uranium (as the $U^{VI}O_2^{2+}$ uranyl ion) phosphate chemistry is vital in the nuclear fuel cycle in separations technologies of used nuclear fuel^[1] and also impacts U^{VI} mobility in the environment.^[2-4] Uranyl phosphate phases have been found in the sediments of contaminated uranium processing facilities^[5,6] and in the subsurface of the Hanford site^[2-4] due to their low aqueous solubilities at circumneutral pHs.^[7] Owing to low solubilities and stable structures, uranyl phosphates have been proposed for environmental remediation strategies^[8] and for potential nuclear waste forms.^[9] The Plutonium Uranium Reduction Extraction (PUREX) process relies on

the coordination of the organophosphate ligand tributyl phosphate to selectively extract U^{VI} and Pu^{IV} from used nuclear fuel dissolved in nitric acid.^[10]

Dominant structure types in inorganic uranyl phosphate crystal chemistry are named for uranyl minerals exhibiting these structural units^[11]—parsonsite,^[12] autunite,^[13] phosphuranylite,^[14] and uranophane.^[15] In the early 2000s significant work was done to obtain high quality single-crystal X-ray diffraction data for uranyl phosphates and structurally similar uranyl arsenates.^[11] Using natural samples or synthetic crystals from gel-diffusion or hydrothermal methods, several uranyl phosphate crystal structures were reported by Locock and Burns that contained the parsonsite-type chain,^[16] autunite-type sheet,^[17–22] phosphuranylite-type sheet,^[23,24] and uranophane topologies.^[25,26] More recently a molten flux crystal growth method has produced several novel uranyl phosphate compounds with phosphuranylite-type sheets or structurally related derivatives.^[27–31] Replacement of the commonly used alkali or alkaline-earth metal cations with organic-based charge-balancing species resulted in uranophane-type structures.^[32,33] Upon heating autunite-type compounds above 130 °C, the autunite sheet reorganizes to the uranophane topology, again highlighting the tendency of uranyl phosphates to adopt one of these four main structural unit types.^[34] There are very few examples where inorganic uranyl phosphate structures deviate significantly from the four main types.^[35,36]

Introduction of organic functional groups to form tri-, di-, and monoalkyl phosphates impacts the coordinating ability of the phosphate anion and influences the overall crystal chemistry of resulting compounds. Most relevant to nuclear fuel reprocessing and PUREX are tributyl phosphate and the radiolytic degradation contaminants di- and monobutyl phosphate. Crystal structures where uranyl ions coordinate only dibutyl phosphate ligands have chain structures different from those observed in parsonsite, while uranyl coordination to dibutyl phosphate, nitrate,

and tributyl phosphine oxide leads to dimeric units.^[37] Organophosphates with shorter carbon chains than butyl (i.e. ethyl and methyl groups) can be useful analogs to study, as they can coordinate and crystallize similar chains^[38] and dimers.^[39,40]

Previously in our group, we used an imidazolium-based ionic liquid with the diethyl phosphate anion to synthesize novel uranyl phosphate compounds with structural units unique to uranyl phosphate chemistry.^[38,41] Here we extend the work by presenting new crystal structures synthesized using the ionic liquids 1-ethyl-3-methylimidazolium dimethyl phosphate and 1-ethyl-3-methylimidazolium dibutyl phosphate (**Figure 1**) to continue exploring how the phosphate organic functional groups impact uranyl crystal chemistry. In conducting ionothermal synthetic reactions, we synthesized and characterized four new uranyl phosphate compounds and discuss the role of the length of the organic functional group in the structures and the chemical system.

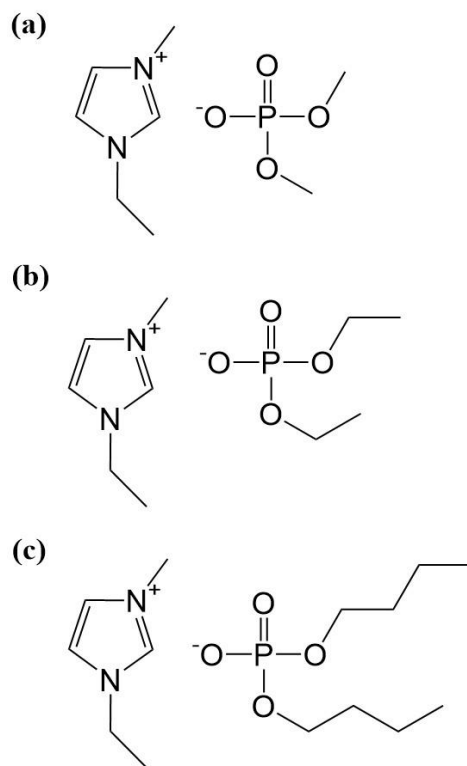


Figure 1. The commercially available ionic liquids (a) 1-ethyl-3-methylimidazolium dimethyl phosphate, (b) 1-ethyl-3-methylimidazolium diethyl phosphate, and (c) 1-ethyl-3-

methylimidazolium dibutyl phosphate that were reactants used in this and previous synthetic studies.

2. Experimental

2.1 Synthesis

Caution! Although depleted uranium was used in the experiments described here, it is radioactive and should only be handled by qualified personnel in appropriate facilities. Uranyl nitrate hexahydrate $\text{UO}_2(\text{NO}_3)_2 \cdot 6\text{H}_2\text{O}$, (ACS Grade 98-102%; International BioAnalytical Industries) was used as received. The ionic liquids 1-ethyl-3-methylimidazolium diethyl phosphate $\text{EMIm-Et}_2\text{PO}_4$ ($\geq 98\%$; Sigma-Aldrich) and 1-ethyl-3-methylimidazolium dibutyl phosphate $\text{EMIm-Bu}_2\text{PO}_4$ (HPLC Grade $\geq 97\%$; Sigma-Aldrich) were used as received. The ionic liquid 1-ethyl-3-methylimidazolium dimethyl phosphate $\text{EMIm-Me}_2\text{PO}_4$ (HPLC Grade $\geq 98\%$; Sigma-Aldrich) was heated slightly to completely liquefy its gel-like consistency at room temperature prior to use. All ionic liquids were shown to be chemically stable when subjected to heat treatments up to $130\text{ }^\circ\text{C}$ without the presence of other reactants as determined by ^1H and ^{13}C NMR (**Figure S7**). Concentrated nitric acid HNO_3 (67-70%; VWR Chemicals BDH), concentrated phosphoric acid H_3PO_4 (85%; EMD Millipore Corp.), and sodium hydroxide NaOH ($\geq 98\%$, beads ACS; VWR Chemicals BDH) were used to prepare 1 M co-solvent solutions. Ultrapure MilliQ water was used for the co-solvent and for preparing stock solutions.

The following ionothermal synthetic parameters were adapted from a previous study.^[42] For each reaction uranyl nitrate hexahydrate (0.1250 g; 0.25 mmol) was measured into a 3 mL Savillex vial, and ionic liquid (0.125 mL) was added for an ideal 2.0 M concentration of U^{VI} in the ionic liquid upon dissolution. The uranyl nitrate did not dissolve in the ionic liquid without application of a heat treatment. If added, co-solvents (0.150 mL) of either MilliQ water, 1 M

NaOH, 1 M H₃PO₄, or 1 M HNO₃ were poured on top. The Savillex vials were sealed and stacked in a Teflon lined 125 mL stainless steel Parr reaction vessel, to which approximately 20 mL of water was added to provide counter pressure during heating. The Parr reaction vessel with contents were heated in a mechanical convection oven using one of two heat treatments. The first included a ramp rate of 1 °C/min up to 80 °C, a soak for 72 hours, and then cooling at 2.5 °C/min to room temperature. The second heat treatment was a ramp up of 1 °C/min to 130 °C, a soak for 24 hours, and then a cooling rate of 0.1 °C/min to room temperature. **Table S1** shows a summary of all the products as determined by X-ray diffraction techniques for each heat treatment, ionic liquid, and co-solvent combination. Optical images of the four new compounds presented below are shown in **Figure S1**. With the described syntheses, each compound except **3** was synthesized in pure form based on powder X-ray diffraction results (**Figure S2**). Quantitative values for yield were not measured, but plenty of material was available for subsequent characterization for each compound.

Compound **1**. UO₂(NO₃)₂·6H₂O (0.1250 g; 0.25 mmol), EMIm-Me₂PO₄ (0.125 mL), and H₂O (0.150 mL) were combined as previously described in a Savillex vial and heated using the method at 130 °C. Colorless tabular crystals were obtained and used for subsequent analysis.

Compound **2**. UO₂(NO₃)₂·6H₂O (0.1250 g; 0.25 mmol), EMIm-Bu₂PO₄ (0.125 mL), and H₂O (0.150 mL) were combined and heat treated to 80 °C. This yielded blade-like crystals of **2**.

Compound **3**. UO₂(NO₃)₂·6H₂O (0.1250 g; 0.25 mmol) and EMIm-Me₂PO₄ (0.125 mL) were measured in a Savillex vial and heated to 130 °C, resulting in tabular colorless crystals.

Compound **4**. UO₂(NO₃)₂·6H₂O (0.1250 g; 0.25 mmol), 0.125 mL EMIm-Me₂PO₄ (0.125 mL), and 0.150 mL 1M HNO₃ (0.150 mL) were mixed in a Savillex vial. **4** crystallized upon cooling after heating at 130 °C.

2.2 Chemical Analysis

Crystals of new compounds were harvested and mounted on double-sided carbon tape that was adhered to an aluminum stub. Chemical analyses were performed using a JEOL JCM-6000PLUS NeoScope Benchtop scanning electron microscope (SEM) equipped with a backscatter electron detector (BED) suitable for energy dispersive X-ray analysis (EDX). SEM images were obtained using a secondary electron detector (SED). EDX spectra confirm the presence of uranium, phosphorus, and nitrogen as shown in **Figure S3**.

2.3 X-ray Diffraction

Crystals with mother liquor were placed in a drop of oil on a microscope slide. Single crystals suitable for X-ray diffraction were picked and mounted onto a cryoloop. Preliminary data collection was performed to obtain a unit cell. For unknown structures a complete sphere of data with frame widths of 0.5° in ω was collected using a Bruker Quazar APEX-II diffractometer equipped with a CCD detector and a MoK_α X-ray source (0.71073 \AA). APEX3 software was used to record the diffraction data and to integrate and apply background, Lorentz, and polarization effect corrections.^[43] SADABS was used for absorption corrections.^[44] Structure solutions were obtained using intrinsic phasing with SHELXT and were refined with SHELXL.^[45,46] Hydrogen atoms were placed in idealized locations using a riding model for organic components or were included for water molecules when located in the difference-Fourier maps. Crystal structure and refinement information is in **Table 1**. Details pertaining to powder X-ray diffraction instrumentation and collection parameters are in **Figure S2**.

Using the obtained structural models, bond valence summations (BVS) were calculated for uranium, phosphorus, and oxygen using bond valence parameters for U(VI)-O and P(V)-O.^[47,48]

The BVS confirmed the oxidation states of the cations and allowed oxygen atom assignment as water molecules or as protonated. The bond valence calculations for each structure are in **Tables S3-S6**.

Table 1. Summary of crystallographic data and refinement parameters.

Compound	1	2	3	4
Chemical Formula	(UO ₂)(H ₂ O)[PO ₂ (OCH ₃) ₂] ₂	(UO ₂) _{1.5} [PO ₂ (OC ₄ H ₉) ₂] ₃	(C ₆ N ₂ H ₁₁)[(UO ₂) _{1.5} (PO ₃ OCH ₃) ₂]	(C ₆ N ₂ H ₁₁)[(UO ₂) ₂ (H ₂ O)(PO ₃ OC ₃ H ₇) ₂ (PO ₂ OCH ₃ OH)]
Formula weight	538.12	1032.62	736.22	997.24
Temperature (K)	120(2)	100(2)	120(2)	100(2)
Crystal system	Monoclinic	Monoclinic	Monoclinic	Monoclinic
Space group	<i>P2₁/c</i>	<i>P2₁/c</i>	<i>P2₁/c</i>	<i>C2/c</i>
<i>a</i> (Å)	11.662(2)	18.960(3)	9.385(2)	20.755(4)
<i>b</i> (Å)	13.410(2)	5.2768(8)	10.142(2)	9.3075(15)
<i>c</i> (Å)	8.4931(14)	36.995(6)	19.587(4)	24.210(4)
α (°)	90	90	90	90
β (°)	103.589(2)	96.969(2)	97.313(3)	101.276(2)
γ (°)	90	90	90	90
<i>V</i> (Å ³)	1291.0(4)	3672.0(10)	1849.2(7)	4586.7(13)
<i>Z</i>	4	4	4	8
ρ_{calc} (g cm ⁻³)	2.769	1.867	2.644	2.888
μ (mm ⁻¹)	12.868	6.802	13.361	14.396
Data Range θ (°)	1.80 – 27.06	1.08 – 26.29	2.10 – 29.00	1.72 – 28.92
Total Reflections Collected	14232	37883	22190	27334
Independent Reflections / Parameters / Restraints	2830 / 171 / 8	7444 / 393 / 0	4612 / 223 / 0	5733 / 296 / 6
<i>R</i> _{int} (%)	4.14	6.32	11.53	6.18
<i>S</i> ^a	1.016	1.043	9.61	1.018
<i>R</i> ₁ , <i>wR</i> ₂ [<i>I</i> > 2 σ (<i>I</i>)] ^{b,c}	2.07, 4.44	3.34, 6.57	4.41, 7.39	3.38, 6.38

R_1, wR_2 (all data) ^{b,c}	3.10, 4.68	4.49, 6.87	10.37, 8.83	6.43, 7.08
---------------------------------------	------------	------------	-------------	------------

$$^a S = \text{Goof} = [\sum w(F_o^2 - F_c^2)^2 / (n - p)]^{1/2}$$

$$^b R_1 = \sum ||F_o| - |F_c|| / \sum |F_o|$$

$$^c wR_2 = [\sum w(F_o^2 - F_c^2)^2 / \sum w(F_o^2)^2]^{1/2}; w = 1/(\sigma^2(F_o^2) + (aP)^2 + bP) \text{ where } P = (\max(F_o^2, 0) + 2F_c^2)/3$$

2.4 Vibrational Spectroscopy

Raman and infrared (IR) spectra were collected for crystals mounted on double-sided carbon tape using an inVia™ confocal Raman microscope from Renishaw and an FT-IR Microscope LUMOS II equipped with a diamond ATR objective, respectively. Raman spectra were measured from 100-1700 cm⁻¹ with an excitation wavelength 785 nm light, while the IR spectra were collected from 600-4000 cm⁻¹. The Raman and IR spectra are in **Figure S4** and **Figure S5**, respectively.

3. Results

3.1 Crystal structures containing chain-based structural units

Compound **1** contains an electroneutral uranyl phosphate heteropolyhedral chain composed of uranyl pentagonal bipyramids and dimethyl phosphate anions (**Figure 2a**). Each uranyl cation is bridged to neighboring uranyl ions through the sharing of two dimethyl phosphate anions. The uranyl pentagonal bipyramidal coordination is completed by a water molecule. The electroneutral chains extend along [100] and are linked by weak van der Waals interactions provided by the methyl groups of the dimethyl phosphate anions (**Figure 2b**). The average uranium to apical oxygen (O_{yl}) bond distance U-O_{yl} and average uranium to equatorial oxygen (O_{eq}) bond distance U-O_{eq} are 1.787(2) Å and 2.377(3) Å, respectively. The average phosphorus to oxygen P-

O bond distance is 1.535(6) Å, and the average carbon to oxygen C-O bond distance is 1.444(8) Å.

Compound **2** contains electroneutral uranyl phosphate chains composed of uranyl square bipyramids and dibutyl phosphate anions (**Figure 2c**). Each uranyl cation is bridged to neighboring uranyl cations through the sharing of two dibutyl phosphate tetrahedra. The chains extend along [010], and the butyl groups provide the necessary bonding to stabilize the overall crystal structure (**Figure 2d**). The average U-O_{yl} and U-O_{eq} are 1.775(1) Å and 2.304(3) Å, respectively. The average P-O bond distance is 1.536(8) Å, the average C-O bond distance is 1.459(2) Å, and the average C-C bond distance is 1.513(7) Å.

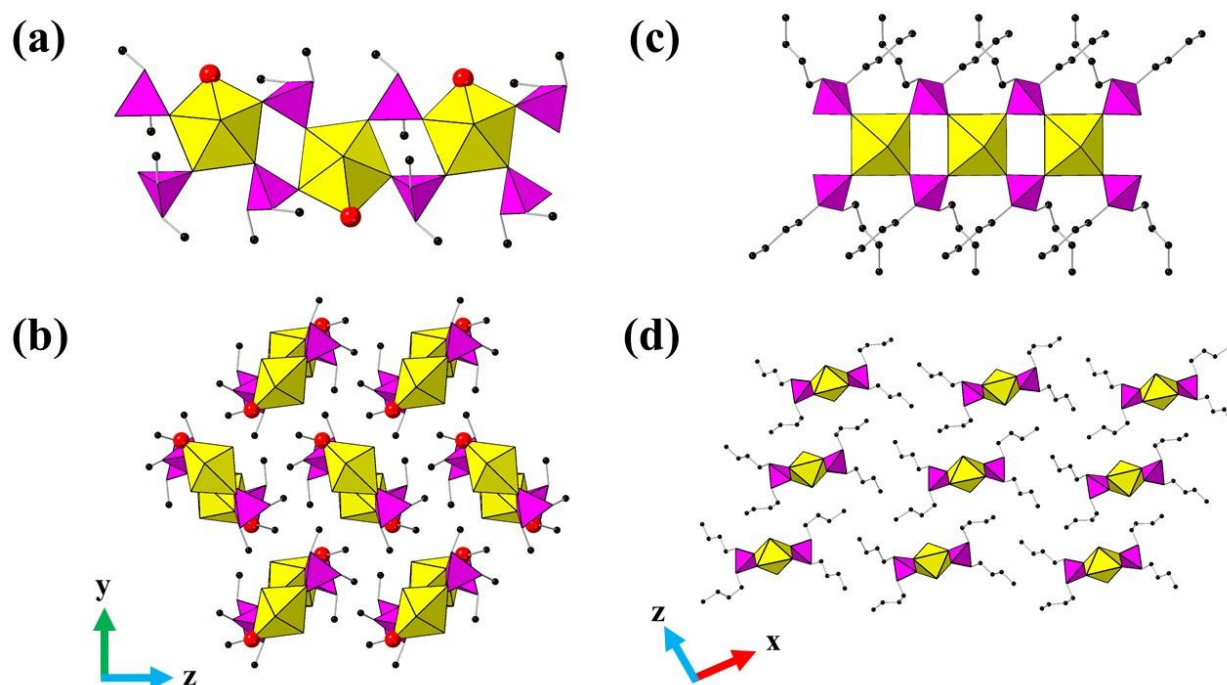


Figure 2. The uranyl phosphate structural unit chains for compounds **1** (a) and **2** (c) and the corresponding crystal packing for **1** (b) and **2** (d). Yellow represents uranyl polyhedra, magenta represents phosphate tetrahedra, red spheres represent water molecule oxygen atoms, and black spheres represent carbon atoms. Hydrogen atoms are omitted for clarity.

3.2 Crystal structures containing sheet-based structural units

Two new uranyl phosphate compounds containing sheet structural units were synthesized using EMIm-Me₂PO₄. In the structure of compound **3**, there is a uranyl phosphate sheet composed of uranyl square bipyramids and methyl phosphate tetrahedra. Each uranyl ion is coordinated to the vertices of four separate methyl phosphate ligands, and where four methyl groups meet, there is a void in the sheet (**Figure 3a**). These sheets lie on (011) and are charge-balanced by the EMIm cations to form the overall crystal structure (**Figure 3b**). The average U-O_{yl} and U-O_{eq} bond lengths are 1.778(6) Å and 2.285(6) Å, respectively. The average P-O, C-O, C-N, and C-C bond lengths are 1.536(12) Å, 1.437(10) Å, 1.38(2) Å, and 1.442(15) Å, respectively.

In the structure of compound **4**, the uranyl phosphate sheet is composed of uranyl pentagonal bipyramids, protonated and unprotonated methyl phosphate tetrahedra, and water molecules (**Figure 3c**). In the sheet, there are dimers of uranyl pentagonal bipyramids formed through the sharing of an equatorial edge. Each uranyl ion within the dimer is coordinated to the vertices of two separate methyl phosphate tetrahedra and one edge-sharing methyl phosphate tetrahedron, the latter of which shares a vertex with the other uranyl ion in the dimeric unit. The vertex-sharing methyl phosphate tetrahedra also share vertices to connect other such uranyl dimers into a chain extending through the sheet along [010]. The final vertex of these tetrahedra along with a free vertex of the dimeric edge-sharing methyl phosphate coordinate a uranyl ion that binds a water molecule and shares the vertices of two separate protonated methyl phosphate tetrahedra. It is through the protonated methyl phosphate tetrahedra that dimeric chains are connected along [101] to form a sheet. These uranyl phosphate sheet structures are linked and charge-balanced by EMIm cations (**Figure 3d**). The average U-O_{yl}, U-O_{eq}, P-O, and C-O bond lengths of the structural unit are 1.768(6) Å, 2.381(6) Å, 1.525(12) Å, and 1.46(4) Å, respectively. The average C-C and C-N bond distances of the EMIm cations are 1.394(19) Å and 1.406(11) Å, respectively.

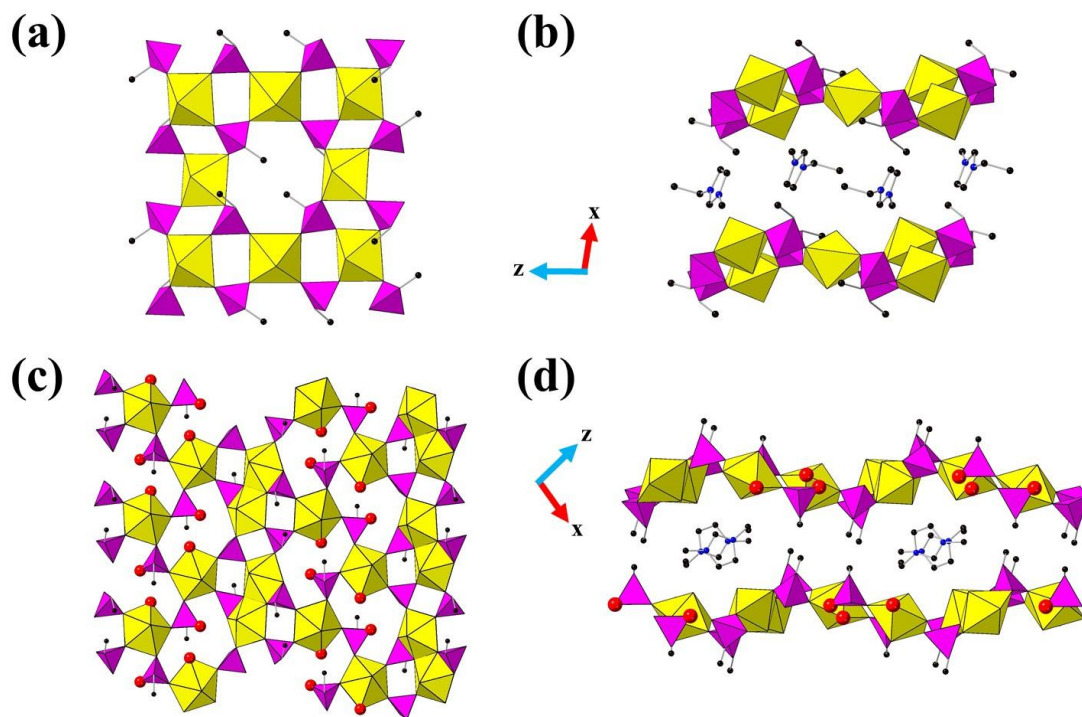


Figure 3. The uranyl phosphate sheet structural unit for compounds **3** (a) and **4** (c), and the crystal packing of two layers of **3** (b) and **4** (d) along the y-axes. Color legend as in **Figure 2** except blue spheres represent nitrogen atoms and red spheres on the phosphate tetrahedra represent protonated oxygen atoms. Hydrogen atoms are removed for clarity.

3.3 Vibrational Spectroscopy

The Raman spectra for all four compounds is dominated by the ν_1 symmetric stretches near 840 cm^{-1} , which is reasonable for uranyl phosphate materials.^[49] The ν_3 asymmetric stretches in the IR spectra are near 910 cm^{-1} for compounds **1**, **3** and **4**, while it is near 929 cm^{-1} for compound **2**. The IR spectra show more prominently than the Raman spectra the bands associated with the organophosphates, protonated oxygen atoms, and EMIm cations, when present. C-H stretches are present at higher wavenumbers $2800\text{--}3200\text{ cm}^{-1}$ with C-H bends near 1450 cm^{-1} . For compounds **3** and **4**, the EMIm cations have stretches due to the imidazole ring near 1570 cm^{-1} .^[50] P-O and O-C stretches ranging from $1000\text{ to }1150\text{ cm}^{-1}$ are attributable to the organophosphate anions.^[51]

Below the uranyl asymmetric stretch are peaks near 800 cm^{-1} that can be attributed to antisymmetric phosphate stretches.^[51]

4. Discussion

4.1 Crystal Structure Comparisons

The four main structure types within uranyl phosphate crystal chemistry are shown in **Figure 4**: parsonsite (or similar chains), autunite, phosphuranylite, and uranophane.^[11] Introduction of organic functional groups such as methyl, ethyl, and butyl on the phosphate anion impacts its coordination capability and results in structural units that depart from the four most commonly observed in inorganic uranyl phosphate compounds.

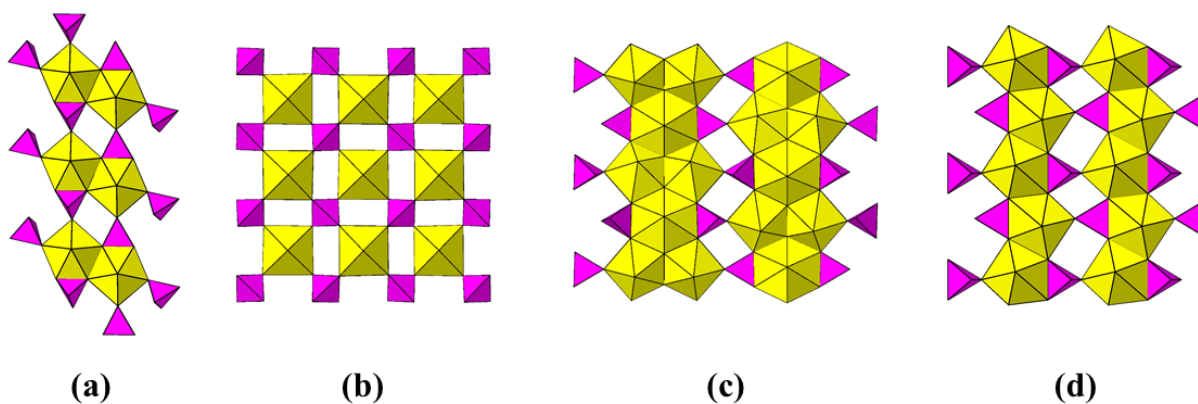


Figure 4. Structural units of the four main families of uranyl phosphate compounds including (a) parsonsite, (b) autunite, (c) phosphuranylite, and (d) uranophane. Figure colors as in **Figure 2** for uranyl and phosphate.

The EMIm-Me₂PO₄ ionic liquid system produced three new crystal structures (compounds **1**, **3**, and **4**). The chain-based structural unit in **1** is quite distinct from that observed in the uranyl phosphate mineral parsonsite.^[12,16] The relative coordination and bonding in **1** is identical to a common topology observed in uranyl sulfate minerals including openheimerite, bobcookite, and

rietveldite^[52–54] as well as organically stabilized uranyl sulfate compounds.^[55–61] Recently, a topologically similar uranyl organophosphate compound was reported in which the water molecules are replaced with trimethyl phosphate.^[62] Compounds **3** and **4** bear slightly greater resemblances to traditional inorganic uranyl phosphate chemistry. The structural unit in **3** has the same topology as the autunite sheet but one quarter of the uranyl positions are vacant due to the presence of the methyl groups. This structure is an analog to the previously synthesized compound in which the monomethyl phosphates are replaced by monoethyl phosphates.^[41] This uranyl monoethyl phosphate analog was synthesized using the ionic liquid EMIm-Et₂PO₄ in a different study,^[41] but it did not form under the synthetic conditions employed here (**Table S1**). The sheet structural unit of **4** is composed of chains similar to that found in the uranyl phosphate mineral lakebogaite,^[63] which has chains similar to parsonsite and of which both can be derived from the parent anion uranophane topology.^[64]

One new crystal structure **2** was synthesized using the EMIm-Bu₂PO₄ ionic liquid system. It contains electroneutral uranyl dibutyl phosphate chain structural units. While the structural unit of **2** was reported earlier, it crystallized in the current study in the monoclinic space group *P*2₁/*c* as opposed to the previously reported triclinic space group *P*-1.^[37] Under different synthetic conditions from those used to synthesize compound **2**, the other uranyl dibutyl phosphate crystal structure was also successfully synthesized (labeled compound **2a** in Supplementary Information). However, compound **2a** was solved in *P*-1 with all angles acute rather than obtuse as reported earlier, where both are acceptable structure solutions (**Table S2**).^[37] This uranyl dibutyl phosphate compound is the main phase identified across a variety of synthetic conditions (**Table S1**). Structurally, **2** is analogous to a uranyl diethyl phosphate compound previously reported by our group,^[38] as well as uranyl phosphates with phenyl phosphate,^[65] phenyl phosphinate,^[66] and

hydroxymethyl phenylphosphinate^[67] rather than the dibutyl phosphate. It was previously noted that the organic functional groups prevent further coordination to other uranyl ions, which would otherwise result in the autunite sheet structure.^[38]

Reactions here using the ionic liquid EMIm-Et₂PO₄ produced no new reportable compounds. Four compounds were identified (**Table S1**), three of which were previously reported^[38] and one that appeared to have a novel unit cell but that diffracted too poorly to obtain an entirely reliable structural model. The preliminary data of the new crystal structure and unit cell parameters are in **Figure S6**. While two studies used EMIm-Et₂PO₄ in syntheses previously, the synthetic conditions were quite different from those utilized here.^[38,41] Syntheses using EMIm-Et₂PO₄ were performed to compare the products with those of the other two ionic liquids to explore the role of the organic functional groups more systematically.

4.2 Heat Treatment Conditions and Resultant Products

We now turn to insights gained regarding the importance of the length of the organic functional groups in stabilizing crystal structures. Overall, 30 reactions incorporated changes in co-solvents with variable pH, heat treatments, and ionic liquid phosphate anion with variable lengths of the organic functional groups. We previously showed that co-solvents can affect topologies of uranyl sulfate structural units in conjunction with different heat treatments that promote crystal growth of kinetically or thermodynamically favored products.^[42] The main focus here was to apply optimal parameters from the previous study to synthesize uranyl phosphate compounds to investigate the role of the ionic liquid anion in crystal structure stabilization. Two general trends emerged as discussed in the next paragraphs.

As described above, heat treatments with soaks at 80°C and 130°C were used. Reactions with EMIm-Me₂PO₄ at 130°C resulted in multiple crystal structures (compounds **3** and **4**) with

solely monomethyl phosphate in the structural unit, which is likely a hydrolysis product of the dimethyl phosphate anion of the original ionic liquid. Reactions with EMIm-Bu₂PO₄ at 130°C resulted in the uranyl dibutyl phosphate chain observed in compound **2**, absent of any hydrolysis product. Finally, with EMIm-Et₂PO₄ at 130°C where the organic chain is intermediate in length between methyl and butyl, a previously reported structure was observed that included a combination of both diethyl and monoethyl phosphate (Sheet **2** in **Table S1**).^[38] These products are the most dominant phases across multiple co-solvent systems for their respective ionic liquids. The first trend is that longer organic chains better prevent hydrolysis at these heat treatment conditions, which we infer is because of the greater hydrophobic nature of the longer carbon chains.

The second crystal chemical trend is observed for compounds **1**, **2**, and Chain **1** previously reported (**Table S1**),^[38] which all contain electroneutral uranyl organophosphate chain-based structural units in which the organic functional groups provide bonding to stabilize the crystal structures (no cationic species charge-balance these structural units). The uranyl dibutyl phosphate compound **2** is the dominant crystalline product in many co-solvent systems under both heat treatments. Chain **1** is an isostructural uranyl diethyl phosphate compound that formed under similar co-solvent systems but only with heat treatments at 80°C for 72 hours with 2.5°C/min cooling. This heat treatment with a lower soak temperature and faster cooling rate produces kinetically favored products.^[42] Because the uranyl dibutyl phosphate compounds form with both heat treatments while the uranyl diethyl phosphate compound does not, it is possible that the butyl groups provide greater stabilization of the crystal structure (i.e. a more thermodynamically favored product) than the ethyl counterparts. In changing the organic functional group to methyls, the uranyl ion adopts a different coordination, topology, and thus crystal packing in compound **1**,

which likely allows the even shorter methyl groups to provide enough van der Waals interactions to stabilize the overall crystal structure. While compound **1** mainly formed at lower temperatures and faster cooling rate environments, it is difficult to confidently state that it is kinetically favored since higher temperatures often hydrolyzed the methyl groups of the dimethyl phosphate anions. Rigorous determination of thermodynamic stability is desirable but outside the scope of the current project. Regardless of the absolute stability of these species, these crystal structures highlight the importance of the organic functional groups.

5. Conclusion

Uranyl phosphate crystal and coordination chemistry is important in mineralogy, the nuclear fuel cycle, and environmental transport of uranium. Here we structurally characterized four new uranyl organophosphates synthesized using ionic liquids. Three new crystal structures were obtained using EMIm-Me₂PO₄ and one new crystal structure was obtained using EMIm-Bu₂PO₄. Two of the crystal structures present unusual topologies with respect to uranyl phosphate chemistry, while the other two are isostructural to similar uranyl organophosphate phases synthesized previously. The length of the organic functional groups impacts the degrees of hydrolysis and influences the coordination and stabilization of the uranyl phosphate phases that formed. In general, longer organic chains prevented hydrolysis from dibutyl phosphate to monobutyl phosphate under higher heat treatment conditions while the shorter organic groups were more prone to hydrolysis, resulting in vastly different uranyl phosphate structures. Furthermore, longer organic groups provided greater van der Waals interactions, leading to more stable products when comparing isostructural compounds. These conclusions are based on the observations of different crystalline structures from various synthetic conditions. Further synthetic endeavors to

obtain more isostructural compounds in conjunction with their thermodynamic data would allow for a more quantitative comparison of these results.

6. Acknowledgments

This work is supported by the Department of Energy, Basic Energy Sciences, Heavy Elements Program under grant number: DE-FG02-07ER15880. Single-crystal X-ray analyses were conducted at the Materials Characterization Facility of the Center of Sustainable Energy at the University of Notre Dame.

CCDC Deposition Numbers 2168258-2168262 contain the supplementary crystallographic data for this paper. This data can be obtained free of charge via <https://www.ccdc.cam.ac.uk/>, or by contacting The Cambridge Crystallographic Data Center, 12, Union Road, Cambridge, CB2 1EZ, UK; fax: +441223336033.

7. References

- [1] T.S. Rudisill, T.C. Shehee, D.H. Jones, G.D. Del Cul, *Sep. Sci. Technol.* **2019**, *54*, 1904–1911. DOI:10.1080/01496395.2019.1578805.
- [2] A. Vázquez-Ortega, N. Perdrial, E. Reinoso-Maset, R.A. Root, P.A. O’Day, J. Chorover, *J. Hazard. Mater.* **2021**, *416*, 126240. DOI:10.1016/j.jhazmat.2021.126240.
- [3] E. Reinoso-Maset, N. Perdrial, C.I. Steefel, W. Um, J. Chorover, P.A. O’Day, *Environ. Sci. Technol.* **2020**, *54*, 6031–6042. DOI:10.1021/acs.est.9b06448.
- [4] W. Um, J.P. Icenhower, C.F. Brown, R.J. Serne, Z. Wang, C.J. Dodge, A.J. Francis, *Geochim. Cosmochim. Acta.* **2010**, *74*, 1363–1380. DOI:10.1016/j.gca.2009.11.014.
- [5] E.C. Buck, N.R. Brown, N.L. Dietz, *Environ. Sci. Technol.* **1996**, *30*, 81–88. DOI:10.1021/es9500825.
- [6] Y. Roh, S.R. Lee, S.K. Choi, M.P. Elless, S.Y. Lee, *Soil Sediment Contam.* **2000**, *9*, 463–486. DOI:10.1080/10588330091134356.
- [7] D. Gorman-Lewis, P.C. Burns, J.B. Fein, *J. Chem. Thermodyn.* **2008**, *40*, 335–352. DOI:10.1016/j.jct.2007.12.004.
- [8] N. Perdrial, A. Vázquez-Ortega, G. Wang, M. Kanematsu, K.T. Mueller, W. Um, C.I. Steefel, P.A. O’Day, J. Chorover, *Appl. Geochem.* **2018**, *89*, 109–120. DOI:10.1016/j.apgeochem.2017.12.001.
- [9] R.C. Ewing, *Proc. Natl. Acad. Sci. U. S. A.* **1999**, *96*, 3432–3439. DOI:10.1073/pnas.96.7.3432.
- [10] D.L. Clark, S.S. Hecker, G.D. Jarvinen, M.P. Neu, Plutonium, in: *The Chemistry of the Actinide and Transactinide Elements*. (Eds. L.R. Morss, N.M. Edelstein, Fuger Jean, J.J. Katz), Springer, **2006**: pp. 813–1264.
- [11] A.J. Locock, *Dissertation*, Univ. of Notre Dame **2004**.
- [12] P.C. Burns, *Am. Mineral.* **2000**, *85*, 801–805. DOI:10.2138/am-2000-5-621.
- [13] J. Beintema, *Recl. Des Trav. Chim. Des Pays-Bas.* **1938**, *57*, (1938).
- [14] F. Demartin, V. Diella, S. Donzelli, C.M. Gramaccioli, T. Pilati, *Acta Crystallogr., Sect. B: Struct. Sci. Cryst. Eng. Mater.* **1991**, *B47*, 439–446. DOI:10.1107/S010876819100099X.
- [15] D.K. Smith Jr., J.W. Gruner, W.N. Lipscomb, *Am. Mineral.* **1957**, *42*, 594–618.
- [16] A.J. Locock, P.C. Burns, T.M. Flynn, *Am. Mineral.* **2005**, *90*, 240–246.

- DOI:10.2138/am.2005.1705.
- [17] A.J. Locock, P.C. Burns, T.M. Flynn, *Can. Mineral.* **2004**, *42*, 1699–1718.
DOI:10.2113/gscanmin.42.6.1699.
- [18] A.J. Locock, P.C. Burns, T.M. Flynn, *Can. Mineral.* **2005**, *43*, 721–733.
DOI:10.2113/gscanmin.43.2.721.
- [19] A.J. Locock, P.C. Burns, *Am. Mineral.* **2003**, *88*, 240–244. DOI: 10.2138/am-2003-0128.
- [20] A.J. Locock, P.C. Burns, M. John, M. Duke, T.M. Flynn, *Can. Mineral.* **2004**, *42*, 973–996. DOI:10.2113/gscanmin.42.4.973.
- [21] A.J. Locock, P.C. Burns, *Can. Mineral.* **2003**, *41*, 489–502.
DOI:10.2113/gscanmin.41.2.489.
- [22] A.J. Locock, W.S. Kinman, P.C. Burns, *Can. Mineral.* **2005**, *43*, 989–1003.
DOI:10.2113/gscanmin.43.3.989.
- [23] A.J. Locock, P.C. Burns, *Can. Mineral.* **2003**, *41*, 91–101.
DOI:10.2113/gscanmin.41.1.91.
- [24] P.C. Burns, C.M. Alexopoulos, P.J. Hotchkiss, A.J. Locock, *Inorg. Chem.* **2004**, *43*, 1816–1818. DOI:10.1021/ic0348547.
- [25] A.J. Locock, P.C. Burns, *J. Solid State Chem.* **2002**, *167*, 226–236.
DOI:10.1006/jssc.2002.9646.
- [26] A.J. Locock, P.C. Burns, *Z. Kristallogr. - Cryst. Mater.* **2004**, *219*, 259–266. DOI:
10.1524/zkri.219.5.259.32744.
- [27] C.A. Juillerat, E.E. Moore, V. Kocovski, T. Besmann, H.C. Zur Loye, *Inorg. Chem.* **2018**, *57*, 4726–4738. DOI:10.1021/acs.inorgchem.8b00434.
- [28] C.A. Juillerat, H.C. Zur Loye, *Cryst. Growth Des.* **2019**, *19*, 1183–1189.
DOI:10.1021/acs.cgd.8b01643.
- [29] V. Kocovski, C.A. Juillerat, E.E. Moore, H.C. Zur Loye, T.M. Besmann, *Cryst. Growth Des.* **2019**, *19*, 966–975. DOI:10.1021/acs.cgd.8b01518.
- [30] C.A. Juillerat, E.E. Moore, T. Besmann, H.C. Zur Loye, *Inorg. Chem.* **2018**, *57*, 3675–3678. DOI:10.1021/acs.inorgchem.8b00302.
- [31] C.A. Juillerat, V. Kocovski, T.M. Besmann, H.C. zur Loye, *Front. Chem.* **2019**, *7*.
DOI:10.3389/fchem.2019.00583.
- [32] R.J. Francis, M.J. Drewitt, P.S. Halasyamani, C. Ranganathachar, D. O'hare, W. Clegg, S.J. Teat, *Chem. Commun.* **1998**, 279–280. DOI:10.1039/A706873E.

- [33] J.A. Danis, J.A. Danis, W.H. Runde, B. Scott, J. Fettinger, B. Eichhorn, *Chem. Commun.* **2001**, 22, 2378–2379. DOI:10.1039/b106916k.
- [34] J.E. Stubbs, J.E. Post, D.C. Elbert, P.J. Heaney, D.R. Veblen, *Am. Mineral.* **2010**, 95, 1132–1140. DOI:10.2138/am.2010.3439.
- [35] G. Morrison, K.A. Pace, H.C. zur Loye, Mild hydrothermal synthesis of potassium uranyl phosphates with layered and framework structures, *J. Solid State Chem.* **2021**, 301, 122293. DOI:10.1016/j.jssc.2021.122293.
- [36] J. Plášil, A.R. Kampf, J. Sejkora, J. Čejka, R. Škoda, J. Tvrđý, *J. Geosci.* **2018**, 63, 265–276. DOI:10.3190/jgeosci.267.
- [37] J.H. Burns, *Inorg. Chem.* **1983**, 22, 1174–1178. DOI:10.1021/ic00150a006.
- [38] T.A. Kohlgruber, S.A. Mackley, F.D. Bo, S.M. Aksenov, P.C. Burns, *J. Solid State Chem.* **2019**, 279, 120938. DOI:10.1016/j.jssc.2019.120938.
- [39] I.A. Charushnikova, A.M. Fedosseev, C. Den Auwer, P. Moisy, *Radiochim. Acta.* **2012**, 100, 173–178. DOI:10.1524/ract.2012.1899.
- [40] B. Kanellakopulos, E. Dornberger, R. Maier, N. Bernhard, H.-G. Stammer, Z.L. Manfred, *Z. Anorg. Allg. Chem.* **1993**, 619, 593–600. DOI:10.1002/zaac.19936190327.
- [41] E.M. Wylie, P.A. Smith, K.M. Peruski, J.S. Smith, M.K. Dustin, P.C. Burns, *CrystEngComm.* **2014**, 16, 7236–7243. DOI:10.1039/c4ce00270a.
- [42] T.A. Kohlgruber, D.E. Felton, S.N. Perry, A.G. Oliver, P.C. Burns, *Cryst. Growth Des.* **2021**, 21, 861–868. DOI:10.1021/acs.cgd.0c01198.
- [43] APEX 3., Bruker AXS Inc., Madison, Wisconsin, USA., 2014.
- [44] SADABS, Bruker AXS Inc., Madison, Wisconsin, USA., 2014.
- [45] G.M. Sheldrick, *Acta Crystallogr., Sect. A: Found. Crystallogr.* **2015**, 71, 3–8. DOI:10.1107/S2053273314026370.
- [46] G.M. Sheldrick, *Acta Crystallogr., Sect. C: Struct. Chem.* **2015**, 71, 3–8. doi:10.1107/S2053229614024218.
- [47] P.C. Burns, R.C. Ewing, F.C. Hawthorne, *Can. Mineral.* **1997**, 35, 155–1570.
- [48] I.D. Brown, D. Altermatt, *Acta Crystallogr., Sect. B: Struct. Sci. Cryst. Eng. Mater.* **1985**, B41, 244–247. DOI:10.1007/s10854-009-0006-1.
- [49] G. Lu, A.J. Haes, T.Z. Forbes, *Coord. Chem. Rev.* **2018**, 374, 314–344. DOI:10.1016/j.ccr.2018.07.010.
- [50] J. Kiefer, J. Fries, A. Leipertz, *Appl. Spectrosc.* **2007**, 61, 1306–1311.

- DOI:10.1366/000370207783292000.
- [51] J. Florián, V. Baumruk, M.S. Trajbl, L. Bednárová, J.S. Těpánek, *J. Phys. Chem.* **1996**, 100, 1559–1568. DOI:10.1021/jp9520299.
- [52] A.R. Kampf, J. Plášil, A. V. Kasatkin, J. Marty, J. Čejka, *Mineral. Mag.* **2015**, 79, 1123–1142. DOI:10.1180/minmag.2015.079.5.8.
- [53] A.R. Kampf, J. Plášil, A. V. Kasatkin, J. Marty, *Mineral. Mag.* **2015**, 79, 695–714. DOI:10.1180/minmag.2015.079.3.14.
- [54] A.R. Kampf, J. Sejkora, T. Witzke, J. Plášil, J. Čejka, B.P. Nash, J. Marty, *J. Geosci.* **2017**, 62, 107–120. DOI:10.3190/jgeosci.236.
- [55] P.M. Thomas, A.J. Norquist, M.B. Doran, D. O’Hare, *J. Mater. Chem.* **2003**, 13, 88–92. DOI:10.1039/b206694g.
- [56] A.J. Norquist, P.M. Thomas, M.B. Doran, D. O’Hare, *Chem. Mater.* **2002**, 14, 5179–5184. DOI:10.1021/cm020793j.
- [57] A.J. Norquist, M.B. Doran, P.M. Thomas, D. O’Hare, *Dalton Trans.* **2003**, 1168–1175. DOI:10.1039/b209208e.
- [58] A.J. Norquist, M.B. Doran, D. O’Hare, *Solid State Sci.* **2003**, 5, 1149–1158. DOI:10.1016/S1293-2558(03)00133-X.
- [59] M.B. Doran, A.J. Norquist, D. O’Hare, *Inorg. Chem.* **2003**, 42, 6989–6995. DOI:10.1021/ic034540j.
- [60] C.L. Stuart, M.B. Doran, A.J. Norquist, D. O’Hare, *Acta Crystallogr., Sect. E: Struct. Rep. Online.* **2003**, E59, m446-m448. DOI:10.1107/S1600536803011966.
- [61] M.B. Doran, B.E. Cockbain, A.J. Norquist, D. O’Hare, *Dalton Trans.* **2004**, 3810–3814. DOI:10.1039/b413062f.
- [62] V. Amani, M. Rafizadeh, *Inorg. Chem. Res.* **2020**, 4, 10–19. DOI:10.22036/icr.2020.232124.1060.
- [63] S.J. Mills, W.D. Birch, U. Kolitsch, W.G. Mumme, I.E. Grey, *Am. Mineral.* **2008**, 93, 691-697. DOI:10.2138/am.2008.2706.
- [64] S. V. Krivovichev, J. Plášil, Mineralogy and Crystallography of Uranium, in: *Uranium Cradle to Grave*, Mineralogical Association of Canada (MAC), Winnipeg, MB, **2013**, pp. 15–119.
- [65] D. Grohol, M.A. Subramanian, D.M. Poojary, A. Clearfield, *Inorg. Chem.* **1996**, 35, 5264–5271. DOI:10.1021/ic960332y.

- [66] D. Grohol, F. Gngl, A. Clearfield, *Inorg. Chem.* **1999**, 38, 751–756.
DOI:10.1021/ic9809761.
- [67] W. Yang, H. Wang, Z.Y. Du, W.G. Tian, Z.M. Sun, *CrystEngComm.* **2014**, 16, 8073–8080. DOI:10.1039/c4ce01172d.